Available online at www.sciencedirect.com
SCIENCE DIRECT
Polymer 47 (2006) 1604–1611
polymer
www.elsevier.com/locate/polymer

Ultra-strong gel-spun UHMWPE fibers reinforced using multiwalled carbon nanotubes

Shilun Ruan [a], Ping Gao [b,*], T.X. Yu [a]

[a] Department of Mechanical Engineering, The Hong Kong University of Science and Technology, Hong Kong, People's Republic of China
[b] Department of Chemical Engineering, The Hong Kong University of Science and Technology, Hong Kong, People's Republic of China

Received 24 October 2005; received in revised form 14 December 2005; accepted 10 January 2006

Abstract

This paper reports the use of multiwalled carbon nanotubes (MWCNT) to reinforce and toughen gel-spun ultra high molecular weight polyethylene (UHMWPE) fibers. By adding 5 wt% MWCNT, ultra strong fibers with tensile strengths of 4.2 GPa and strain at break of ~5% can be produced. In comparison with the pure UHMWPE fiber at the same draw ratios, these values represent increases of 18.8% in tensile strength and 15.4% in ductility. In addition, a 44.2% increase in energy to fracture has also been observed. The mechanism of reinforcement has been studied using a combination of high resolution scanning electron microscopy (SEM) and micro-Raman spectroscopy. Carbon nanotube alignment along the tensile draw direction has been observed at high elongation ratios. Such alignment induces strong interfacial load transfer both at small and large strains to enhance the stiffness and tensile strength of the composite fiber. Consequently, the mechanical properties of the composite fiber follow closely with the rule of mixtures. Our work also reveals potential for positive deviation from rule of mixtures if the CNT alignment can be further optimized.

Keywords: Gel-spun MWCNT/UHMWPE nanocomposite fibers; CNT alignment; Load transfer

1. Introduction

High performance ultrahigh molecular weight polyethylene (UHMWPE) fibers with Young's modulus >90 GPa and tensile strength >3 GPa and strain at break up to 5% were first developed in 1980 by Smith et al. [1]. These fibers quickly found applications in various fields from helicopters to tennis rackets and from ballistic-resistant garments to nautical sea ropes, replacing other fibers such as Kevlar and carbon fibers [2]. However, applications of these fibers in structural composites have been limited by some less favorable properties of the materials, such as creep under static conditions, and poor shear modulus and strength [3].

Carbon nanotubes (CNTs) are considered to be perfect whiskers with exceptional mechanical properties. It is generally accepted that the tensile strength and modulus of individual CNTs are up to 150 GPa and 1 TPa, respectively [4]. CNTs are also known to have extremely high resilience with ultimate strain at break greater than 5%. It is believed that incorporation of CNTs in polymer matrix may lead to ultimate fiber reinforcement nanocomposites with significantly enhanced mechanical properties. A large number of papers have been published on the reinforcement of polymer composites using CNTs, but results are mixed [5–13].

We were amongst the first groups to report the use of CNTs in a highly oriented polymer matrix to investigate toughening effects in the homopolymer [14]. By incorporating 1 wt% MWCNTs into highly oriented UHMWPE films, a 150% increase in strain energy absorption before failure under tensile loading and a 25% increase in tensile strength has been achieved. Micro-Raman spectroscopic analysis of the composite fiber under loading has shown multi-scale interactions between the highly aligned UHMWPE molecules and the embedded MWCNT. It has been observed that at intermediate strains, the MWCNTs act as slippage sites, allowing the matrix to deform without significant bond stretching. However, these sites act as pseudo taut tie molecules at large strains to produce the strain hardening effects that are absent from the highly anisotropic pure UHMWPE films.

The primary objective of this report is to demonstrate the simultaneous reinforcing and toughening effects of CNTs on the highly oriented gel-spun UHMWPE fibers. Mechanisms of

* Corresponding author. Tel.: +852 2358 7126; fax: +852 2358 0054.
E-mail address: kepgao@ust.hk (P. Gao).

0032-3861/$ - see front matter © 2006 Elsevier Ltd. All rights reserved.
doi:10.1016/j.polymer.2006.01.020

reinforcements are also studied by Micro-Raman and microscopy analysis.

2. Experimental

2.1. Sample preparations

MWCNTs from Carbon Nanotech Point (Shenzhen, China) were treated using the mixture of concentrated H_2SO_4 and HNO_3 [14]. Scanning electron micrographs displaying the morphology of the acid treated MWCNTs are shown in Fig. 1. Fig. 1(a) and (b) were obtained without and with gold sputtering coating, respectively. Little difference in diameter can be observed by gold sputtering, as both micrographs show a similar diameter size and range. It can be seen from Fig. 1 that the acid treated CNTs display a range of diameters and lengths with the mean diameter ~30 nm and a length of up to several microns. Prior to use, all acid treated CNTs were first dispersed into ethanol and supersonicated for 3-h. This CNT-ethanol mixture was then poured into the mixture of 3 wt% UHMWPE in decalin. The mixture was further stirred magnetically for about 1 h and then fed into a single screw extruder with the metering and capillary zone temperatures at 180 and 135 °C, respectively. The solution after flowing through a capillary die of 1 mm diameter and a length to diameter ratio of 30 was then quenched into water at ambient temperature to form gel fibers. After complete drying, the fibers containing 5 wt% MWCNT were hot pressed at 120 °C for 30 min to form precursor fibers. These pressed fibers were then hot drawn to the predefined draw ratios (here, 30) by a two-stage drawing. The precursor fibers were drawn to a draw ratio of 5 at 120 °C in the first stage and then to the draw ratio of 30 at 130 °C.

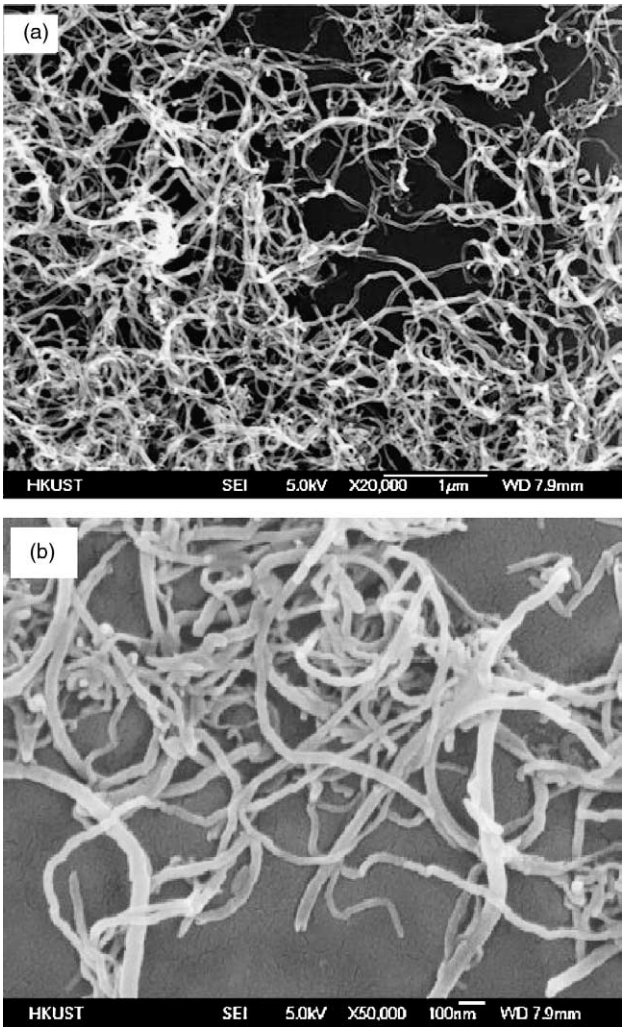

Fig. 1. High resolution scanning electron microscope photographs for the acid-treated MWCNTs. (a) The CNTs were directly photographed without any gold coating; and (b) The CNTs were sputtered coated with a thin layer of gold.

Tensile tests were carried out on a MTS RT/5 micro tester with a load cell of 10 N at room temperature and an elongation rate of 2.54 mm min^{-1}. The precursory fibers were stuck to the paper board frame using CN glue. The highly drawn fibers were wound around a small smooth needle and fixed by rubber grip system to minimize any fiber slippage or damage. For all specimens, cross-sectional areas were determined by the weighing method on long fibers of 1 m in length. The density of the 5 wt% composite was estimated as 995 kg m^{-3} by assuming that the densities of the pure UHMWPE and MWCNT at 970 and 2000 kg m^{-3}, respectively.

2.2. Differential scanning calorimetry

Differential scanning calorimetry (DSC) was carried out on a Pyris 1 DSC at the standard heating and cooling rates of 10 °C min^{-1}. The tests were carried out on the as prepared gel-spun precursor fibers and the drawn fibers at a draw ratio of 30 containing 0 and 5 wt% MWCNT.

2.3. Micro-Raman spectrometry

The micro-Raman spectroscopy experiments were performed on a Renishaw Ramanscope 1000 using the argon laser at 514 nm in conjunction with a micro-strain tester. Details can be found in Ruan et al. [14]. The measurements were performed using the backscattering geometry and the samples were the fibers of pure UHMWPE and 5 wt% composites at a draw ratio of 30.

3. Results

3.1. Mechanical properties

Fig. 2(a) shows the tensile drawing responses of the compacted precursor fibers measured at room temperature. Tests were performed on at least five different specimens for each composition, and the average tensile properties together with the standard deviation are summarized in Table 1. The 5 wt% MWCNT composite fibers show a significant increase in ductility of ~34% and an increase of energy to fracture of 64% in comparison with the pristine UHMWPE fibers. These are consistent with our earlier report [14]. The major difference here is the magnitude of the tensile moduli, which are significantly higher than that of the precursor films reported

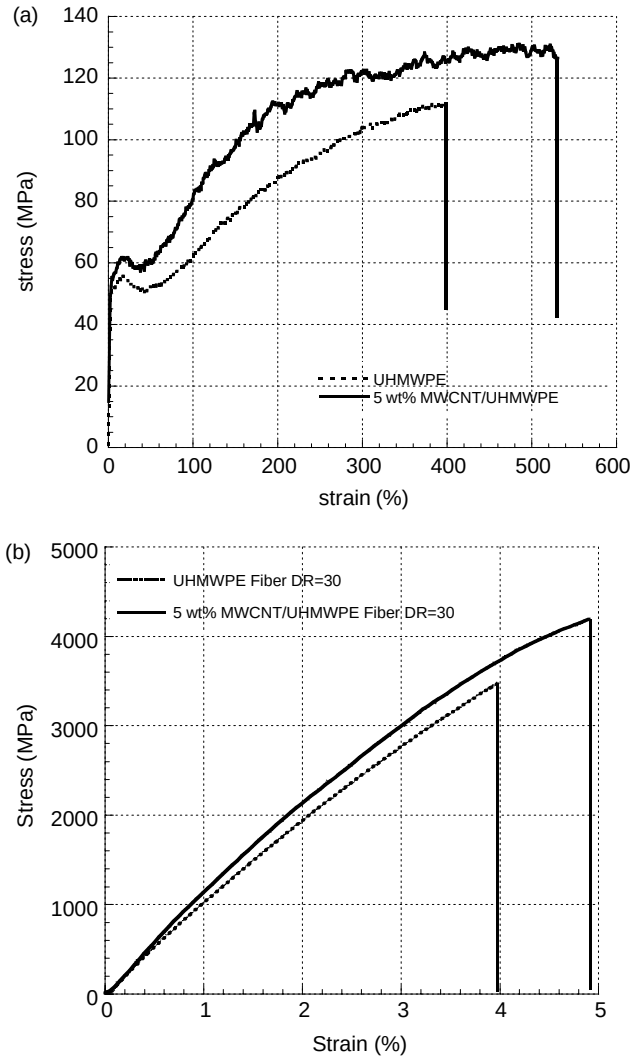

Fig. 2. Tensile stress–strain curves measured at a cross-head speed of 25 mm min^{-1} at room temperature. (a) The precursor fibers after compaction at 120 °C; and (b) The highly oriented fibers at DR = 30.

in our previous publication. The difference arises from the fact that these fibers were partially oriented during the gel-spinning process.

The most remarkable observations were made on the tensile properties enhancement in the highly aligned composite fibers containing 5 wt% MWCNTs. Fig. 2(b) shows the typical stress–strain curve of the 5 wt% MWCNT/UHMWPE composite fiber at a draw ratio of 30 measured at a cross-head speed of 25 mm min^{-1} at room temperature. The data on pure UHMWPE fibers are also shown here. Clearly, the addition of MWCNTs leads to enhancements in tensile strength, tensile modulus and the ductility of the drawn fiber. Measurements were performed on at least five specimens and the average properties together with standard deviations are summarized in Table 2. It should be noted that the data scattering amongst each measurement is very small. The 5 wt% MWCNT/UHMWPE fiber shows tensile modulus of 136.8 GPa, tensile strength of 4.2 GPa and strain at break of 4.7%, representing enhancements of 11.6, 18.8 and 15.4%, respectively, in comparison with the pure UHMWPE fiber. These are the most outstanding properties ever achieved through gel spinning process at 3 wt% UHMWPE concentrations. Even higher tensile modulus and tensile strength up to 180 and 6 GPa have been reported in UHMWPE fibers drawn from single crystal mats [15]. However, it is not commercially viable to produce fibers from single crystal mats that have to be prepared from extremely dilute solutions.

These properties also represent the highest mechanical properties amongst all ultra-strong fibers reported so far. Table 3 lists the mechanical properties of typical commercial high performance fibers [16]. Clearly, the composite fiber developed in this study shows the highest tensile strength, ductility and energy to fracture.

Theoretical predictions on the mechanical properties of nanocomposites are still in their infancy. To a first order approximation, the rule of mixture model developed for micromechanics has been widely used [17]. Mathematically, the rule of mixture for the strength and modulus of the composite can be represented by

$$\varepsilon^*_{PE} < \varepsilon^*_{NT}$$

$$\sigma^*_C = \begin{cases} \eta\phi_{NT}\sigma'_{NT} + (1-\phi_{NT})\sigma^*_{PE} & \text{for low } \phi_{NT} \\ \eta\phi_{NT}\sigma^*_{NT} & \text{for high } \phi_{NT} \end{cases} \quad (1)$$

and

$$E^*_C = \begin{cases} \eta\phi_{NT}E^*_{NT} + (1-\phi_{NT})E^*_{PE} & \text{for low } \phi_{NT} \\ \eta\phi_{NT}E^*_{NT} & \text{for high } \phi_{NT} \end{cases} \quad (2)$$

where ε, σ, E, η and ϕ are the ultimate strain at break, tensile strength, tensile stiffness, effectiveness parameter, and volume fraction, respectively. The subscripts PE and NT represent the properties of the matrix UHMWPE and dispersed MWCNTs, respectively. The superscripts * and $'$ refer to the ultimate and maximum property values, respectively. The effectiveness parameter η varies from 1 for the unidirectional reinforcement to 5/8 for reinforcement in two-dimensional random orientations.

Table 1
Tensile properties of precursory fibers

	Modulus (GPa)	Yielding stress (MPa)	TS (MPa)	EAB (%)	Energy to fracture (MPa)
UHMWPE	2.42 ± 0.40	54.5 ± 1.8	114.6 ± 2.1	402.0 ± 20.1	361.8 ± 22.9
5 wt% MWCNT	2.62 ± 0.32	60.4 ± 4.5	132.7 ± 3.9	540.4 ± 104.7	593.2 ± 114.5

EAB, strain at break; TS, tensile strength.

Table 2
Mechanical properties of the highly oriented fibers at DR = 30

	Modulus (GPa)	TS (GPa)	EAB (%)	Energy to fracture (MPa)
UHMWPE	122.6 ± 1.9	3.51 ± 0.13	4.03 ± 0.15	76.7 ± 7.5
5 wt% MWCNT	136.8 ± 3.8	4.17 ± 0.04	4.65 ± 0.35	110.6 ± 10.5

EAB, strain at break; TS, tensile strength.

Table 3
Comparison of mechanical properties of various commercial high performance fibers [13] and 5 wt% MWCNT/UHMWPE fiber

Property	E-glass	S-glass	Type I carbon	Type III carbon	Kevlar 49	Spectra 900	UHMWPE (5 wt% CNT)
Density (g/cm^3)	2.54	2.49	1.7–1.8	1.85–1.96	1.45	0.97	0.995
Tensile strength (GPa)	2.4	4.5	3–5.6	2.4	3.6	3.0	4.2
Elongation at break (%)	3–4	5.4	1.0–1.8	0.38–0.5	2.8	3.5	4.65
Young's modulus (GPa)	72.4	85	235–295	345–520	135	117	136.8
Specific tensile strength (10^4 m)	9.6	18.5	17.3–33.7	12.2–13.3	25.3	31.5	43.1
Specific young's modulus (10^4 m)	291	348	1331–1770	1950–2868	950	1231	1403
Specific energy to fracture (10^3 m)	1.32	4.97	0.68–2.88	0.26–0.72	3.72	7.56	11.3[a]

Maximum energy to fracture calculated by $E\varepsilon^2/2$.
[a] Experimentally measured in this work.

In order to apply the rule of mixtures, mechanical properties of MWCNTs and the pure UHMWPE fiber are required. For the latter, the experimentally measured properties are used, i.e. at DR = 30, $E_{PE} = 122.6$ GPa, $\sigma_{PE} = 3.51$ GPa, $\varepsilon_{PE} = 4\%$. On the other hand, a wide range of values obtained through molecular dynamics simulations (MD) and direct experimental measurements are available [18–20]. The values obtained by MD simulations are generally higher than those measured experimentally. The recently reported experimental results [21] appear to be consistent with the MD results and are used here: $E_{NT} = 910$ GPa, $\sigma_{NT} = 150$ GPa, $\varepsilon_{NT} = 12\%$. The volume fraction of the MWCNTs inside the 5 wt% composite fiber may be estimated to be 2.5%. Using these data together with $\eta = 5/8$ in Eqs. (1) and (2) gives $\sigma_c^* = 4.18$ GPa and $E_c^* = 133.8$ GPa, respectively. These are in almost perfect agreement with our experimentally measured values shown in Table 2.

3.2. Reinforcement mechanism

In order to elucidate the reinforcing mechanism, a combination of differential scanning calorimetry (DSC), scanning electron microscopy (SEM) and micro-Raman spectroscopy were also performed on the highly oriented fibers.

DSC analysis on the precursor fibers and fibers at DR = 30 was performed on a Pyris DSC. The data on the composite were obtained on the 5 wt% MWCNT/UHMWPE fibers. The thermograms in Fig. 3 clearly show that the PE crystallization temperature increases due to the addition of MWCNT. This becomes more apparent as the PE alignment increases. The highly drawn composite fiber shows a crystallization temperature of 117.8 °C, which is 5.3 °C higher than the pristine fiber at the same draw ratio. The drastic increase in the PE crystallization temperature strongly suggests that the MWCNT has the nucleating effects on PE crystals, particularly in the highly aligned fibers [22]. On the other hand, the crystallinity of the composite fibers is slightly lower than that

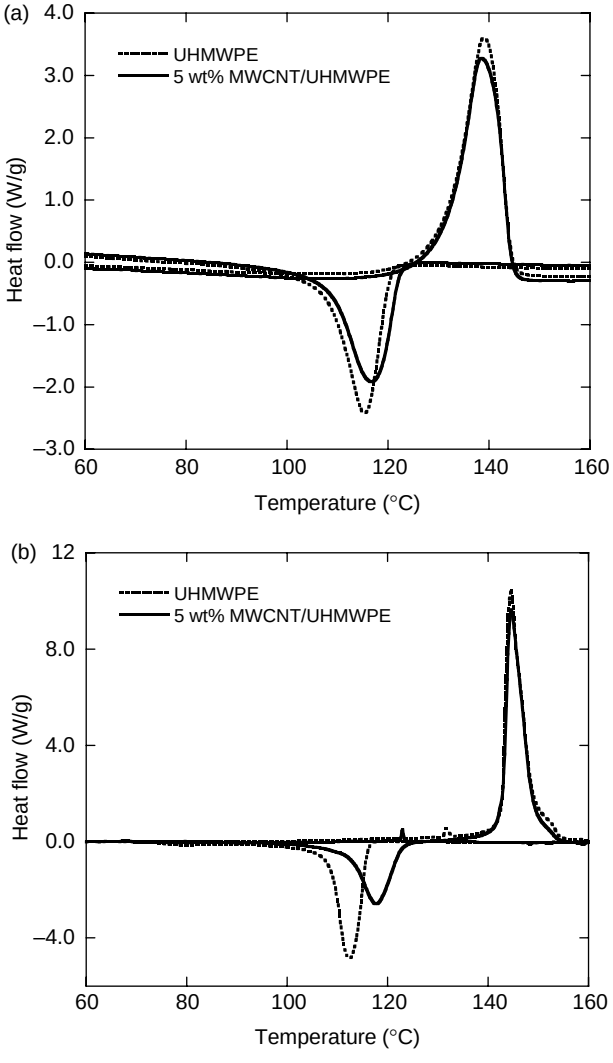

Fig. 3. DSC thermograms on the precursor and draw fibers at (a) DR = 1, and (b) DR = 30. The heating and cooling rates used were 10 °C min^{-1}.

of the pristine fibers by about 5%. The highly drawn PE fiber shows a high crystallinity of 98%.

Fig. 4 shows the scanning electron micrographs of the cross sections of the 5 wt% composite fibers at DR = 1 at two different magnifications. It is seen clearly that dispersion of CNTs inside the UHMWPE matrix is of multiscale. Most of the CNTs were dispersed in the form of 1 μm diameter clusters, while some were dispersed as individual tubes. An arrow A is labeled towards one of these singly dispersed tubes. Some of the clusters are of elliptical shapes indicating some orientation effect during the gel spinning and solid state compression processes. It is also of interest to note that nearly all the clusters exist in the middle of the fiber, which explains why it is hard to find any CNTs if we take a direct SEM image on the fiber surface. A detailed examination of the cluster reveals that the CNTs are intimately mixed with the matrix PE. A clearer illustration of this is shown in the magnified micrograph obtained close to the region indicated by arrow B. The result is consistent with our earlier observations on the precursor films [14], where intimate mixing of CNTs with the UHMWPE matrix was also observed in the dense cluster regions. It is worthwhile to mention that similar dispersion phenomena was observed in the nanocomposite of HA/UHMWPE where the HA nanoparticles are dispersed into domains of HA rich and HA depleted regions [23]. In the HA rich regions, the HA nanaoparticles are also intimately mixed with the UHMWPE matrix. What is important to note is that such large CNT clusters do not hinder the drawability of the composite fiber. In fact, it appears that such clusters may even facilitate higher drawability.

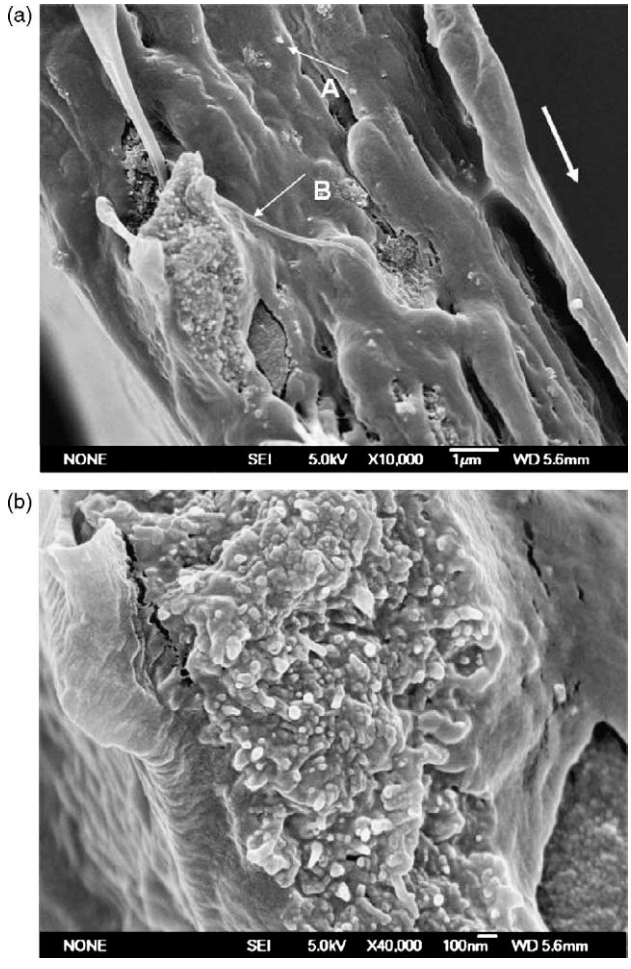

Fig. 4. High resolution scanning electron micrograph on the cross section of the 5 wt% MWCNT/UHMWPE composite. (a) Global view of the cross section, and (b) a magnified view of the region indicated by arrow B to show the intimate mixing effect of the CNTs inside the dense cluster. The fiber axis is indicated by the arrow inserted on the top right hand side corner of the micrograph (a).

Stricking changes in the morphology of the composite fiber occur at draw ratios above 25. At such high draw ratios, in situ CNT alignments along draw direction during hot draw can be observed. The development of CNTs alignment is a consequence of CNTs pulling out from the cluster region at high draw ratios. This is illustrated in Fig. 5. The micrographs were obtained on the surface of a 5 wt% MWCNT/UHMWPE fiber at a draw ratio 30. A global feature of the fiber containing one CNT cluster is shown in Fig. 5(a), and the magnified view

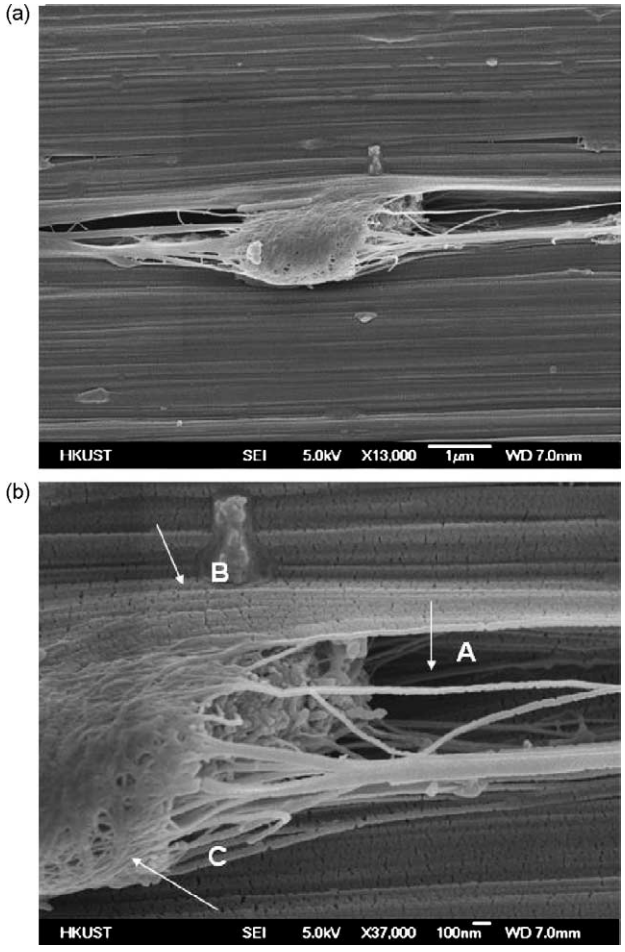

Fig. 5. High resolution scanning electron micrographs on the fiber surface of the 5 wt% MWCNT/UHMWPE at DR = 30. The fiber axis is horizontal. (a) A global view of the fiber surface enclosing one large CNT cluster on the surface. (b) A magnified view of the fiber close to the CNT cluster showing the orientation of CNTs due to hot draw. Individual CNT alignments along the fiber axis can be readily observed, and these tubes can be seen clearly to have been pulled out from the cluster due to hot draw at high draw ratios. Thus the originally dense cluster as shown in Fig. 4 becomes loose.

around the CNT cluster is shown in Fig. 5(b). It should be noted that the occurrence of a cluster of CNT rich region on the exterior of the fiber surface is a rare event. As mentioned before, most of the CNT clusters have a tendency to stay away from the exterior surface. The exposure of such CNT clusters to the outer surface may be caused by the significant reductions in the cross-section of the composite fiber at high draw ratios. A number of intriguing features can be observed in Fig. 5(b). Firstly, a number of filaments of the diameter ranging from 30 to 100 nm are pulled out from the CNT cluster. Some of the filaments join together after having been pulled out to form a bundle. This suggests that some of the filaments were a mixture of CNTs with the UHMWPE matrix. Individual CNT pulling out and alignment can also be observed. To facilitate observation, arrow A is inserted to point to two of such individual tubes, one of them is a long curved loop that was formed by separation from the joint filament during pulling out. The diameter of the CNTs measured from the cross section (Fig. 4(b)) is of 20–50 nm and these pulling out fibers are also of the diameters of ~30 nm. These values are in excellent agreement with those observed on the SEM micrographs of the pure CNTs in Fig. 1(b) and (c). The lengths of the individual CNT filaments are at least 3 μm as can be seen from Fig. 5(a). A closer examination behind the arrow A leads to the discovery of a number of individual tubes that have been pulled out from the cluster to align along the fiber direction. Secondly, there is an apparently strong interfacial interaction at the interface of the CNT cluster and the UHMWPE matrix. This is seen through the interfacial shear deformation of the cluster as indicated by arrow B. Thirdly, the pulling out effect of the filaments results in the cluster region becoming a loose network structure. Within the loose cluster, one may clearly see the intimate mixing of CNTs with the PE matrix where individual CNTs may be readily observed. Finally, within the loose cluster, the CNTs are aligned predominantly along the draw direction with some oriented perpendicular to the draw direction as indicated by arrow C.

We can confidently claim that this is the first report to demonstrate the CNT alignment inside a highly aligned matrix. We are also the first group to show the development of such alignment through CNT pulling out from dense CNT clusters due to interfacial load transfers. In the meantime, strong load bearing effect may be expected from the embedded CNTs. Direct evidences confirming interfacial load transfer were obtained using micro-Raman spectroscopy as shown below.

The interfacial load transfer was investigated using micro-Raman spectroscopy on the 5 wt% composite fiber and the pure UHMWPE fiber at a draw ratio 30. Fig. 6 depicts the Raman shift versus strain for the asymmetric C–C stretching band of PE (1060 cm^{-1}) and G-band of carbon nanotubes. The G-band has been deconvoluted to two peaks at 1595 and 1612 cm^{-1} using a combination of Lorenzian and Gaussian functions. The major band shift at 1595 cm^{-1} was used for analysis. Fig. 6(a) shows the G-band Raman shift versus strain for CNTs in the 5 wt% composite fiber. We may divide the data into three regions according to the nature of the deformation in the composite fiber. This is similar to what was done in our previous paper [14]. The Raman shift at strains less than 1.5% is labeled as region I, corresponding to the nearly elastic deformation of the composite fiber. In this region, a steep linear red-shift in the G-band of the CNTs can be observed. A straight line is fitted to the data in this region and superimposed onto the experimental data. This is followed by region II where intensive red–blue shift is observed. This region is, however,

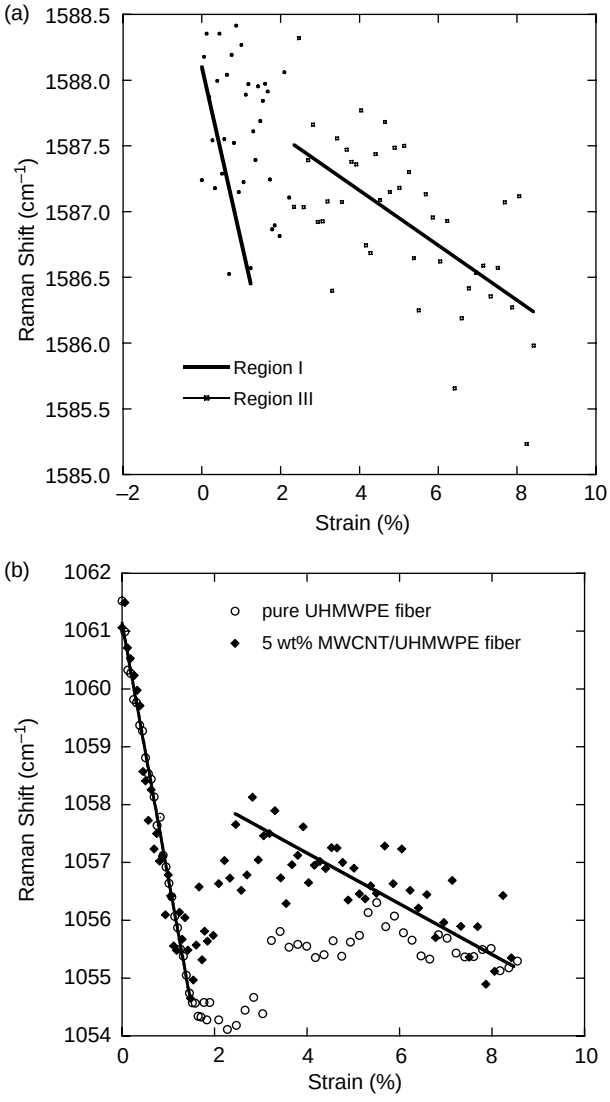

Fig. 6. Raman shift versus strain for the asymmetric C–C stretching band of PE (1060 cm^{-1}), and the G-band (1595 cm^{-1}) of CNT inside the 5 wt% MWCNT/UHMWPE composite fiber at draw ratio = 30. The Raman shift of the pure UHMWPE fiber at draw ratio is also shown. (a) Raman shift of the G-band of MWCNTs inside the 5 wt% MWCNT/UHMWPE composite fiber at DR 30 versus applied strain. The data are divided into three regions. In region I, the G-band shows a rapid linear shift until the applied strain reaches 1.5%. Between strains of 1.5 and 2%, the CNTs experience stick and slip and the G-band shows an intensive red–blue shift and is considered as region II. At higher strains, the CNTs withstands a continuous tension during deformation and a second linear red-shift regime is observed in the G-band of the CNTs, and denoted as region III. (b) Raman shift of the asymmetric C–C stretching band (1065 cm^{-1}) as a function of strain for the pure and 5 wt% composite fiber at DR = 30. The data on the composite fiber mirror that of the CNTs in (a). The pure UHMWPE fiber shows no strain hardening after the initial linear deformation.

very narrow and appears to complete at 2% strain. At strains above 2%, region III can be identified where the CNTs inside the composite fiber experiences continuous tension during loading.

The data scattering, particularly in region I, deserves further analysis. In fact, this is a common phenomena observed in many polymer nanocomposites containing MWCNTs. Some have attributed to the multiwall characteristics of the CNTs [21,24]. However, the micrographs depicted in Fig. 5 strongly suggest that such scattering is caused by the orientation distribution of CNTs inside the composite. As can be seen close to arrow C, some CNTs are aligned normal to the draw direction. These CNTs will experience compression rather than tension during deformation. As the Raman spectrum is an average response over a domain size of ~1 μm diameter, if the Raman scattering was averaged over domains of randomly orientations of CNTs (see arrow C, Fig. 5(b)), the measured Raman shift will be nearly zero with respect to the unstressed sample. An apparently lower red-shift will also be observed if the laser spot was focused around the partially oriented regions, see the interface between the cluster and the aligned CNTs in Fig. 5(b). To reduce scattering, polarized Raman microscopy should be conducted.

The overall response of the PE matrix in the composite fiber also follows closely with that of the CNTs. A three region response can also be identified. At strains less than 1.5%, the matrix shows a linear red-shift. A strong yield is observed at this strain to give a temporary stick-slip response until 2% strain. At strains greater than 2%, i.e. in region III, the matrix undergoes a clear strain hardening response. These results are again consistent with our earlier work on the composite films [14]. Except that the red-shift in the elastic region is much larger. The total red-shift is seven wavenumbers, whereas the films showed a total red-shift of three wavenumbers in the linear region. This is of course reasonable since the modulus here is 100% higher than that of the films.

The C–C bonds in the pure PE fiber displays very similar Raman shifts to those in the composite fiber in the linear region or strains less than 1.5%. The major difference lies in the stick and slip responses in the pure PE fiber. Apparently, after the onset of yield, the C–C bond experiences no further stretching at higher strains. Again, these observations are consistent with our earlier findings in the drawn films [14].

In our previous paper [14], we proposed that the enhanced ductility in the composite fiber was caused by higher chain mobility of PE chains close to the dispersed CNTs. The abrupt blue shift inside the PE matrix within region II also evidently supports this argument. Apparently, there is a strong slip of PE chains at strains about 1.5% to facilitate the configurational change in order to sustain larger deformations. The major difference here is the rapid strain hardening effect that succeeds this softening effect in region II.

4. Conclusions

We have successfully demonstrated that adding MWCNTs can lead to super strong and ductile UHMWPE composite fibers. A simultaneous toughening and strengthening effect has been observed in these composite fibers. These properties will make gel-spun UHMWPE even more competitive in the area of high energy absorption applications such as in ballistic vests. This is clearly illustrated in Table 3 where the 5 wt% MWCNT/UHMWPE composite fibers show the highest specific tensile strength and energy to fracture amongst all commercial high performance fibers.

The strong interfacial interaction between the dispersed MWCNTs and the matrix PE has been demonstrated through DSC, SEM and micro-Raman spectroscopy. The CNTs act as nucleating sites for PE crystal growth. In situ CNT orientation along the fiber direction occurs through CNT pulling out from the micron-sized CNT dominated clusters at high draw ratios. The elongated CNTs are dispersed as individual tubes or bundles of a few CNTs intimately surrounded by the UHMWPE matrix. Raman spectroscopy confirms that such conformations of CNT reinforce the UHMWPE matrix both in terms of stiffness and tensile strength. The stiffness is enhanced through load bearing effect at small strains and the tensile strength is enhanced by strain hardening effect on the matrix.

The tensile modulus and strength of the composite fiber appear to show very good agreement with the predictions of the rule of mixtures. Some positive deviations have been observed in this study. As not all the CNTs are aligned with the matrix PE, further alignment or better dispersion of CNTs may lead to more positive deviations from the rule of mixtures.

Acknowledgements

The project was funded by the Research Grant Council of Hong Kong under a CERG grant HKUST 6159/04E and DSM Research, the Netherlands. We are particularly grateful to the fruitful discussions with Dr Harm ver der Werff, Performance Materials, DSM research.

References

[1] Smith P, Lemestra PJ, J Mater Sci 1980;15:505–514.
[2] Lemstra PJ, Kirschbaum R, Ohta T, Yasuda H. In: Ward IM, editor. Developments in oriented polymers-2. New York: Elsevier Applied Science Publishers; 1987 [chapter 2].
[3] Peijs AAJM, Rustidge AD, de Kok JJM, Rijsdijk HA. In: Verpoest I, Jones F, editors. Interfacial phenomena in composite materials '91'. Oxford: Butterworth-Heinemann; 1991. p. 34.
[4] Iijima S. Nature 1999;354:56–8.
[5] Alan BD, Collins S, Munoz E, Rzazl JM, Ebron VH, Ferraris JP, et al. Nature 2003;423:703.
[6] Gong X, Liu J, Baskaran S, Voise RD, Young JS. Chem Mater 2000;12:1049.
[7] Weisenberger MC, Grulka EA, Jacques D, Rantell T, Andrews R. J Nanosci Nanotech 2003;3(6):535–9.
[8] Andrews R, Weisenberger MC. Curr Opin Solid State Mater Sci 2004;8:31–7.
[9] Bai JB. Carbon 2003;41:1325–8.
[10] Barber AH, Cohen SR, Wagner HD. Appl Phys Lett 2003;82(23):4140–2.
[11] Choi YK, Gotoh Y, Sugimoto K, Song S, Yanagisawa T, Endo M. Polymer 2005;46(25):11489–98.

[12] Kim GM, Michler GH, Pvtschke P. Polymer 2005;46(18):7346–51.
[13] Tatro SR, Clayton LM, O′Rourke Muisener PA, Rao AM, Harmon JP. Polymer 2004;45(6):1971–9.
[14] Ruan SL, Gao P, Yang XG, Yu TX. Polymer 2003;44:5643–54.
[15] Kanamoto T, Tsuruta A, Tanaka K, Takeda M, Porter RS. Macromolecules 1988;21:470.
[16] Kim JK, Mai YW. Engineered interfaces in fiber reinforced composites Amsterdam; Newyork: Elsevier Sciences; 1998.
[17] McCrum NGL, Buckley CP, Bucknall CB. Principles of polymer engineering. Oxford University Press, New York 1988.
[18] Demczyk BG, Wong YM, Cumings J, Hetman M, Han W, Zettal A, et al. Mater Sci Eng 2002;A334:173–8.
[19] Wagner HD, Lourie O, Feldman Y, Tenne R. Appl Phys Lett 1998;72(2):188–90.
[20] Srivastava D, Wei C, Cho K. Appl Mech Rev 2003;56(2):215–30.
[21] Wood JR, Zhao Q, Wagner HD. Composites Part A 2001;32:391.
[22] Sandler JKW, et al. Polymer 2004;45(6):2001–15.
[23] Fang L, Leng Y, Gao P. Biomaterials 2005;26(17):3471.
[24] Schadler LS, Giannaris SC, Ajayan PM. Appl Phys Lett 1998;73(26):3842.